PHOTONICS Research

Revelation of the birth and extinction dynamics of solitons in SWNT-mode-locked fiber lasers

YUDONG CUI[1] AND XUEMING LIU[1,2,3,*]

[1]State Key Laboratory of Modern Optical Instrumentation, College of Optical Science and Engineering, Zhejiang University, Hangzhou 310027, China
[2]Institute for Advanced Interdisciplinary Research, Nanjing University of Aeronautics and Astronautics, Nanjing 210016, China
[3]School of Physics and Electronic Science, Hunan University of Science and Technology, Xiangtan 411201, China
*Corresponding author: liuxueming72@yahoo.com

Received 16 November 2018; revised 8 January 2019; accepted 26 January 2019; posted 29 January 2019 (Doc. ID 352214); published 13 March 2019

The dispersive Fourier transform (DFT) technique opens a fascinating pathway to explore ultrafast non-repetitive events and has been employed to study the build-up process of mode-locked lasers. However, the shutting process for the mode-locked fiber laser seems to be beyond the scope of researchers, and the starting dynamics under near-zero dispersion remains unclear. Here, the complete evolution dynamics (from birth to extinction) of the conventional soliton (CS), stretched pulse (SP), and dissipative soliton (DS) are investigated by using the DFT technique. CS, SP, and DS fiber lasers mode locked by single-walled carbon nanotubes (SWNTs) are implemented via engineering the intracavity dispersion map. The relaxation oscillation can always be observed before the formation of stable pulse operation due to the inherent advantage of SWNT, but it exhibits distinct evolution dynamics in the starting and shutting processes. The shutting processes are dependent on the dispersion condition and turn-off time, which is against common sense. Some critical phenomena are also observed, including transient complex spectrum broadening and frequency-shift interaction of SPs and picosecond pulses. These results will further deepen understanding of the mode-locked fiber laser from a real-time point of view and are helpful for laser design and applications.

https://doi.org/10.1364/PRJ.7.000423

1. INTRODUCTION

Mode-locked fiber lasers delivering ultrafast pulses have been employed in numerous applications as diverse as ophthalmology, micromachining, medical imaging, and precision metrology [1–3] because fiber lasers have several inherent advantages, e.g., high electrical efficiency, lower maintenance, higher reliability, smaller footprint, and easier transportability [4,5]. So far, fiber lasers have generally been implemented with passively mode-locked techniques, such as nonlinear polarization rotation (NPR), nonlinear optical loop mirrors, semiconductor saturable absorber mirrors (SESAMs), single-walled carbon nanotubes (SWNTs), and two-dimensional semiconductor materials [6–11]. Among them, SWNTs are the most promising candidate for ultrashort pulse generation because they possess ultrafast excited state carrier dynamics and high optical nonlinearity [8,12].

To pursue higher pulse energy, researchers successively proposed the conventional soliton (CS), stretched pulse (SP; also named dispersion-managed soliton), and dissipative soliton (DS) by engineering intracavity group velocity dispersion (GVD) [7,13]. The dynamics of the mode-locked fiber laser and its output features depend mainly on the dispersion map of a laser oscillator [13–16]. Soliton fiber lasers are generally constructed with an anomalous-dispersion condition, and pulses can be sustained through the balance of nonlinear and dispersive phase shifts [11]. So it is called a CS to distinguish it from other types of solitons in mode-locked fiber lasers [17]. When the net dispersion is near zero, a SP forms, which can decrease intracavity nonlinearity by periodically stretching and compressing [14,17]. Under net-normal or all-normal cavity dispersion, the pulse-shaping dynamics is dominated by gain and loss with the assistance of dispersion, nonlinearity, and spectral filtering [7]. DSs are always highly chirped, so that they can hold higher pulse energy and nonlinear phase shift [18]. In fact, each kind of pulse possesses unique features that are useful for specific applications. CSs are easy to obtain and compatible with transmission in single-mode fiber (SMF) [11]. SPs have a wide spectral width and low phase noise, and have been employed in numerous applications [1,14]. The high-energy pulse based on DSs greatly promotes the development of high-power ultrafast lasers [7].

A real-time oscilloscope is the common tool to record the temporal evolution process, while the spectral information and pulses close to even overlapping each other cannot be resolved due to the limited electronic bandwidth [2,19–22]. Achieving a temporally and spectrally resolved study of the transient dynamics is always a challenge because every transient event possesses a singular occurrence with unique spectro-temporal features. The recently developed time-stretch dispersive Fourier transform (TS-DFT) technique provides a powerful way for real-time, single-shot measurements of ultrafast phenomena [23]. This technique helps scientists to experimentally resolve the evolution of femtosecond soliton molecules [24–26], the dynamics of soliton explosions [27], and pulsating solitons [28,29]. The TS-DFT technique was also employed to measure the build-up process of solitons [2,25,30–35]. These works focus mainly on the starting dynamics of solitons [2,31], soliton molecules [25,33], and multi-pulse operation [36] in the mode-locked fiber laser under anomalous dispersion. The spectral build-up process of DS in the net-normal dispersion regime was reported in a recent work [32]. However, the starting dynamics of SPs has not been studied experimentally, whether in the temporal of spectral domain. The investigation of the build-up process among CSs, SPs, and DSs is an attractive topic, which can help to explain how the obviously distinct pulses are generated. Moreover, the studies about the starting dynamics of passive mode-locking lasers have helped researchers understand build-up time, capability of self-starting, and Q-switched instability, which is crucial to applications [19–22]. Additionally, the evolution dynamics when mode-locked fiber lasers are shut down also remains unclear. Circulating pulses can be amplified by thousands of times in the relaxation time of the gain fiber after the pump power is switched off, as the roundtrip time is far less than the relaxation time. Moreover, the turn-off time is generally more than several milliseconds. As a result, pulses in mode-locked lasers may not experience extinction directly, as is generally believed.

In this work, the entire evolution dynamics (from starting up to shutting down) of an SWNT-mode-locked fiber laser is measured via the TS-DFT technique. By managing intracavity net dispersion, CSs, SPs, and DSs are achieved under negative, near-zero, and positive dispersion conditions in the mode-locked laser, respectively. Their starting and shutting processes can be obtained with high-speed photodetectors and a real-time oscilloscope. The build-up processes of CSs, SPs, and DSs include the relaxation oscillation, quasi-mode locking, and stable pulse operation stages, but they display distinct transient evolution dynamics. CSs, SPs, and DSs also experience different dynamics and energy fluctuations when the laser is shut down. Several new physical evolution processes are observed in the measurement, and these results are helpful for in-depth understanding of the mode-locked fiber laser.

2. EXPERIMENTAL SETUP

Figure 1 shows the schematic diagram of the SWNT-mode-locked fiber laser and the measurement scheme. The oscillator consists of an SWNT-based mode locker, a ∼7 m-long erbium-doped fiber (EDF) with ∼4 dB/m absorption at 980 nm, a wavelength-division-multiplexed coupler (WDM), an optical coupler, a polarization-independent isolator (PI-ISO), and a polarization controller (PC). A 980-nm laser diode (LD) provides pump via a 980/1550-nm WDM. An optical switcher is placed between the LD and WDM to switch the laser on or off. A coupler with a 10% output port is used to extract pulses from the cavity, and the PI-ISO ensures unidirectional operation. The PC is utilized to optimize the mode-locking performance by adjusting the cavity linear birefringence. The fabrication procedure and parameters of the SWNT-based mode locker can be found in Ref. [37]. ∼10 m of SMF is inserted into the cavity to adjust the net dispersion. The dispersion parameters of the EDF and SMF are about −20 and 17 ps/(nm · km) at 1550 nm, respectively.

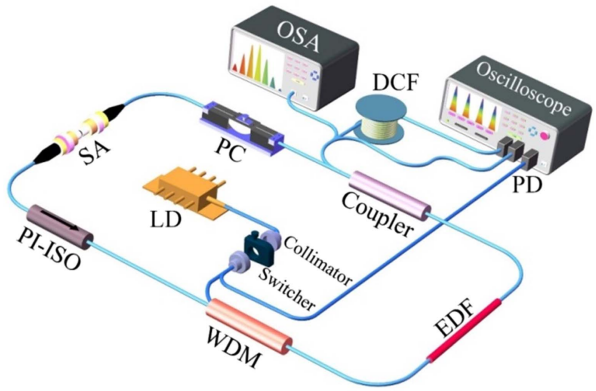

Fig. 1. Schematic diagram of the experimental setup. EDF, erbium-doped fiber; PC, polarization controller; LD, laser diode; SA, saturable absorber; WDM, wavelength-division-multiplexed coupler; PI-ISO, polarization-independent isolator; OSA, optical spectrum analyzer; DCF, dispersion compensation fiber.

First, ∼17 m SMF is in the cavity, and the cavity length is ∼24 m. The roundtrip time is 118.96 ns and the net dispersion is negative of ∼ − 0.2 ps^2. In this case, CSs with typical Kelly sidebands can be achieved [11]. Then, SMF is gradually cut short carefully to adjust the cavity dispersion to be near zero. In this case, the cavity length is ∼17 m with a roundtrip time of 83.92 ns, and the dispersion is ∼ − 0.004 ps^2. Finally, the inserted SMF is removed from the cavity, and only the pigtails of the devices remain. The total cavity length remains ∼14 m. The roundtrip time and intracavity net dispersion are 69.28 ns and ∼0.02 ps^2, respectively. By managing intracavity dispersion, CSs, SPs, and DSs are achieved in the SWNT-mode-locked fiber laser.

The real-time temporal detections for solitons are recorded with two high-speed photodetectors and a real-time oscilloscope. The real-time spectral information can be obtained by dispersing pulses in an ∼5 km dispersion-compensating fiber (DCF) prior to detection. The spectral information could be mapped into the temporal waveform via DCF. The time-averaged spectra are measured via an optical spectrum analyzer (OSA). When the switcher is set as on or off, the pump power can be transmitted or blocked. As a result, the fiber laser can be started up or shut down. In order to monitor the starting and shutting dynamics of the mode-locked fiber laser, a part of the pump power is split and used as the triggering signal of the oscilloscope, as shown in Fig. 1. As a result, only about

60% of the pump power from the LD can be coupled into the gain fiber via the WDM. The threshold values of the pump power for generation of CSs, SPs, and DSs are 32 mW, 42 mW, and 52 mW, respectively. However, CSs, SPs, and DSs are measured at 36 mW, 50 mW, and 58 mW, respectively.

3. RESULTS AND DISCUSSION

Figure 2 demonstrates the whole spectral evolution dynamics for an SWNT-mode-locked fiber laser under distinct dispersion conditions. The starting and shutting processes of CSs, SPs, and DSs are shown in Figs. 2(a), 2(b), and 2(c), respectively. Benefitting from the SWNT SA, relaxation oscillation can be observed, and the unstable stage prior to soliton formation is completely suppressed [25,38]. As a result, the start-up processes in Fig. 2 are similar to our previous results [38], including relaxation oscillation, quasi-mode-locking stage, and stable soliton operation, while obvious different evolution profiles of intensity can be observed due to the different laser cavity parameters (e.g., the length of fiber, SA, and gain coefficient) and initial conditions (e.g., pump power and initial noise). In Fig. 2(a), the laser spike of quasi-mode locking here is much stronger, and relaxation oscillation with about 1 ms is longer. Relaxation oscillation is defined as the duration from the first laser spike beginning to the last spike ending prior to the formation of mode locking. When pump power is blocked, CS pulses can last ~0.3 ms continuously and then vanish rapidly. This may be attributed to the mode locker whose loss increases exponentially as pulse energy decreases.

In the left part of Fig. 2(b), the formation of SPs takes ~1 ms with relaxation oscillation of ~0.8 ms. But after that, periodical intensity fluctuation lasts ~4.5 ms. The modulation may originate from relaxation oscillation, as the period at the beginning (from −5 ms to −4 ms) is identical to that of relaxation oscillation. In fact, relaxation oscillation can induce periodical lasing in the build-up process of mode-locked lasers [25]. However, it needs more time to quiet down the instability for SPs. The shutting process for SPs on the right side of Fig. 2(b) displays distinct evolution dynamics in comparison with CSs [Fig. 2(a)]. The intensity of SPs is modulated intensively before pulses vanish, which is the result of the common interaction of the EDF and SA (this is also a kind of *Q*-switched instability). The mechanism is explained as follows.

When the pump is blocked, the pulse energy first decreases along with the pump power. Pulses experience lower gain, and the loss of the mode locker can become larger with smaller pulse energy. At a certain time when intracavity loss is beyond the gain, the intracavity energy may decline abruptly. The following pump power can still induce the accumulation of population inversion. After a period of time, gain may be larger than loss again, which can lead to the increase of intracavity energy. It is similar to the process of *Q*-switching. It should be noted that the evolution dynamics can be influenced by many other factors, e.g., pump intensity, turn-off time, and SA. Here, one SWNT SA is used in the experiment, and the pump intensity for SPs is slightly larger than for CSs. The turn-off time can be set from hundreds of nanoseconds to several milliseconds. Owing to the larger pulse energy, narrower pulse width, and larger pump power, it is easier for SPs to be re-amplified in the shutting process. For CSs, it is hard to circulate again when the turn-off time is short, as shown in Fig. 2(a). With longer turn-off time, CSs generally vanish quickly first, and SPs experience longer *Q*-switched instability. When the turn-off time is several milliseconds longer than the relaxation time of gain fiber, the shutting dynamics of CSs is shown in Fig. 3. The pulse intensity decreases gradually at the beginning, and pulses vanish sharply when the pulse energy is lower than a certain value. Then a lasing spike can be observed after ~1.5 ms, which is the accumulation process of population inversion. However, lasing cannot be achieved again because the gain is less than the intracavity loss after the lasing spike. However, the fluctuation can be shortened and even suppressed completely with the faster turn-off time and suitable cavity design.

For DSs, the evolution in the starting process seems to be similar to CSs, except that one lasing spike is much stronger, as shown on the left side of Fig. 2(c). This may result from the shorter cavity length and higher pump power. Hence relaxation oscillation is longer at ~1.5 ms, whose characteristics are determined by the cavity structure and pump power [39]. The shutting process of DSs on the right side of Fig. 2(c) exhibits obvious intensity fluctuation, but a different evolution intensity envelop than the SPs in Fig. 2(b), because of the distinct pulse energies, widths, and evolution traces.

The data in Fig. 2 exhibited along the time axis are segmented with respect to the corresponding roundtrip time,

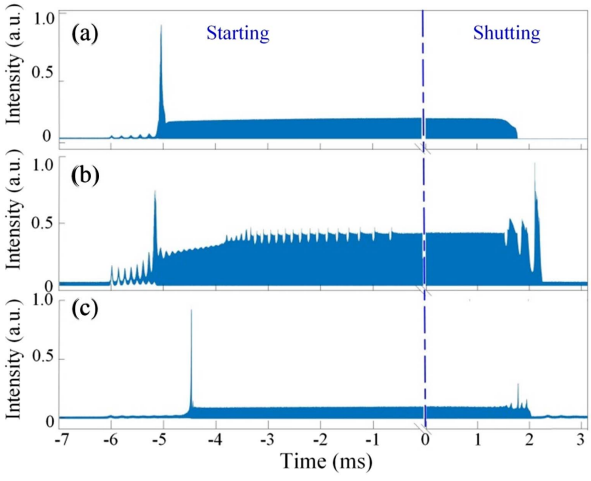

Fig. 2. Real-time observation of starting (left) and shutting (right) processes for (a) CSs, (b) SPs, and (c) DSs. These are the detection results of the oscilloscope after transmission in DCF. The relative coordinates are used for time and intensity.

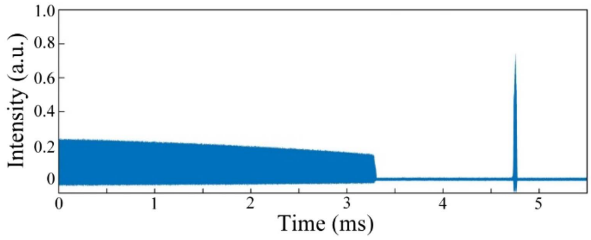

Fig. 3. Shutting process of CSs when the turn-off time is more than 5 ms. This is the direct measuring result without DFT.

and the buildup dynamics of solitons is depicted with the roundtrip time and roundtrip number simultaneously. The real-time evolution dynamics of CSs, SPs, and DSs are shown in Figs. 4, 5, and 7, respectively. The mapping relationship between the spectral and temporal domain can be expressed as $\Delta t = |D|L\Delta\lambda$, where $\Delta\lambda$ is the spectral spacing, Δt is the time spacing, and D and L are the dispersion parameter and length of DCF, respectively [23,25]. Since D is about -160 ps/(nm · km) and L is ~5 km in our experiments, the relationship can be expressed as $\Delta t = 0.8$ ns/nm × $\Delta\lambda$. The bandwidths of the CSs, SPs, and DSs are 6.5 nm, 13 nm, and 9 nm, corresponding to about 5 ns, 10 ns, and 7 ns in the temporal domain. Note that the evolution dynamics is not shown under the whole roundtrip time in Figs. 4, 5, and 7 for the sake of aesthetics, as the SPs are still much smaller than the roundtrip time.

A. Starting and Shutting Dynamics for CS Fiber Lasers

The experimental data in Fig. 4 are from Fig. 2(a), which shows the starting and shutting dynamics for CSs in the SWNT-mode-locked fiber laser. As in previous results [2,25], beating dynamics is first formed with the spectrum widening, and then the laser experiences a complex multi-pulse spectrum evolution, as shown in Figs. 4(d) and 4(e). In particular, the complex multi-pulse spectrum can broaden in an extremely short time, which corresponds to the strong lasing spike in Fig. 1(a). Finally, the complex multi-pulse state collapses and forms the stable single-soliton operation. The complex pulse and energy evolution reflect the variation of gain, which is related to the population inversion in EDF [39]. The longer EDF in this work can lead to strong gain oscillation. Strong amplification can lead to the transient high peak power inducing the strong self-phase modulation and abrupt spectral broadening. CSs cannot maintain the single-pulse operation state. From the shutting process in Fig. 4(b), the decaying process of solitons can be resolved clearly. As the pulse energy decreases, the spectral width and intensity become smaller. The sidebands depart from the central wavelength gradually and disappear at a certain position. Figure 4(c) shows the spectra of CSs measured by the OSA and the single-shot spectrum measured via the DFT technique. The real-time single-shot spectrum agrees quite well with the time-averaged optical spectrum, highlighting the mapping relationship linked by dispersion [25]. The experimental observations show that the spectra have obvious Kelly sidebands, which are the typical characteristics of solitons [40].

B. Starting and Shutting Dynamics for SP Fiber Lasers

Figure 5 shows the starting and shutting dynamics for SPs, corresponding to Fig. 2(b). Beating dynamics also exists in the build-up process of SPs shown in Figs. 5(a) and 5(e). It should be noted that the evolving SP is accompanied by two subordinate pulses, as shown in Figs. 5(a) and 5(c). The subordinate pulses are also generated via beating dynamics. The spectral bandwidth and energy of SPs increase gradually after the beating dynamics, which is different from CSs [Fig. 4(a)]. In Figs. 5(a) and 5(c), we can observe that obvious periodical modulation is displayed along the roundtrip, even for the remaining subordinate pulses. The modulation starts from the relaxation oscillation and evolves continuously to the formation of a stable SP, which can be seen in Figs. 2(b) and 5(a). It can be inferred that the modulation stems from the gain variation induced by relaxation oscillation. Additionally, there is an interaction process between SPs and a picosecond pulse. As shown in Figs. 5(a) and 5(f), the wavelength of the picosecond pulse evolves periodically along the roundtrip. During the process, the intensity of picosecond pulses changes periodically, while SPs remain almost unchanged. From the zoom-in typical results in Fig. 6, we can clearly see that, when the energy becomes larger (smaller), the wavelengths of the picosecond pulses move toward (away from) the central wavelength of the SP. The spectral and temporal shutting dynamics are shown in Figs. 5(b) and 5(d), respectively. Corresponding to the fluctuation in

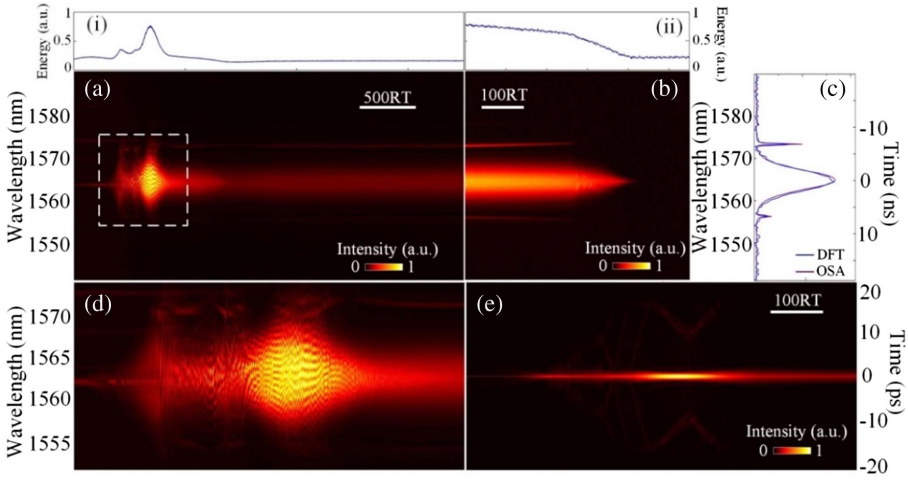

Fig. 4. Starting and shutting dynamics for the CS fiber laser. (a) Real-time spectral evolution dynamics during the formation of CSs. (b) Real-time spectral evolution dynamics during the shutting for CSs. (i) and (ii) show the energy evolution corresponding to (a) and (b), respectively. (c) Optical spectra of solitons measured by the OSA and DFT technique. (d) Close-up of the data in the square of (a), revealing the interference pattern for the beating dynamics and the complex multi-pulse evolution. (e) Fourier transform of each single-shot spectrum corresponds to the field autocorrelation of (d). RT: roundtrip.

Figs. 2(b) and 5(d), the spectral width and intensity change, as shown in Fig. 5(b). Note that SPs operate in an unstable manner during the shutting process due to the drastic change in population inversion. Figure 5(g) shows the spectra of SPs measured by the OSA and DFT techniques, and they show similar profiles with a smooth Gaussian shape. These are the typical characteristics of SPs [7,14].

C. Starting and Shutting Dynamics for DS Fiber Lasers

Figure 7 shows the starting and shutting dynamics for DSs, corresponding to Fig. 2(c). The spectra broaden in a short time along with the rapid increase of intracavity energy. Some interference fringes can be observed at this stage in Fig. 7(a), which is distinct from the beating dynamics in Figs. 4 and 5. A series of typical spectra is extracted from Fig. 7(a) and depicted in Fig. 7(e) along with the roundtrip. The single-shot spectra at both edges have evident fringes that could be generated when the pulse energy of the DS is large enough [7]. Then the spectral width broadens and compresses along with the rise and fall of energy, and finally a stable DS forms. During the shutting process, the spectral width and intensity of DSs show oscillation, as shown in Figs. 4(b) and 4(d), due to variation in the gain. In fact, the remaining population inversion can still provide gain within the relaxation time of doped ions. But it is difficult to drive stable operation. Figure 7(f) shows the spectra of DSs measured by the OSA and DFT techniques, and they both show similar rectangular profiles, which is one of the features of DSs [7].

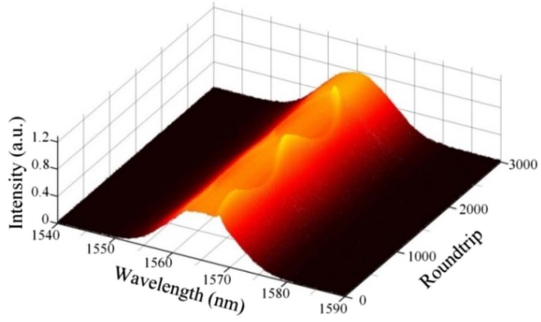

Fig. 6. Interaction of SPs and picosecond pulses. Data are from Fig. 5(f).

D. Discussion

These results are obtained in SWNT-mode-locked fiber lasers by engineering the intracavity dispersion map. Under anomalous, near-zero, and normal dispersion, mode-locked fiber lasers can generate CSs, SPs, and DSs, respectively. The difference in the birth and extinction dynamics for CSs, SPs, and DSs should be attributed to the distinct pulse characteristics (e.g., pulse energy) and pump powers. It should be noted that the results depend on the used mode locker, which has the capability of self-starting. Similar results can also be achieved with mode lockers with low saturable intensity, e.g., SESAMs, while mode lockers with high saturable intensity, e.g., NPR, can induce a divergent evolution path. When the

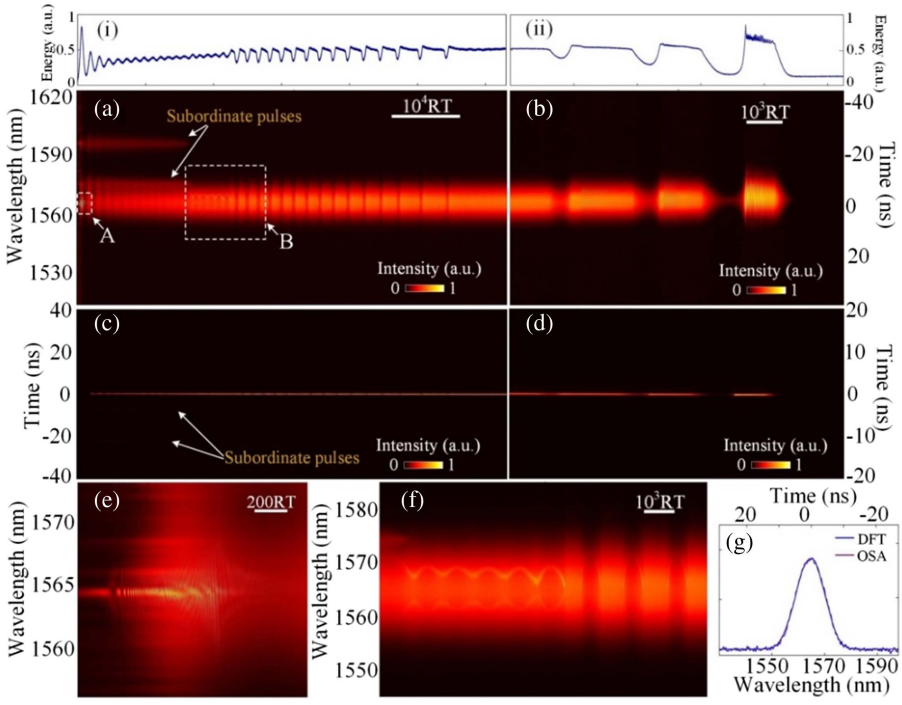

Fig. 5. Starting and shutting dynamics for the SP fiber laser. (a) Real-time spectral evolution dynamics during the formation of SPs. (b) Real-time spectral evolution dynamics during the shutting process for SPs. (i) and (ii) show the energy evolution corresponding to (a) and (b), respectively. Experimental real-time observation without DFT for the (c) starting and (d) shutting processes, corresponding to (a) and (b), respectively. Results with and without DFT display a time difference due to the delay of DCF. (e) Close-up of the data from region A in (a), revealing the interference pattern for the beating dynamics. (f) Interaction of SPs and picosecond pulses. The data are from region B in (a). (g) Optical spectra of SPs measured by the OSA and DFT technique.

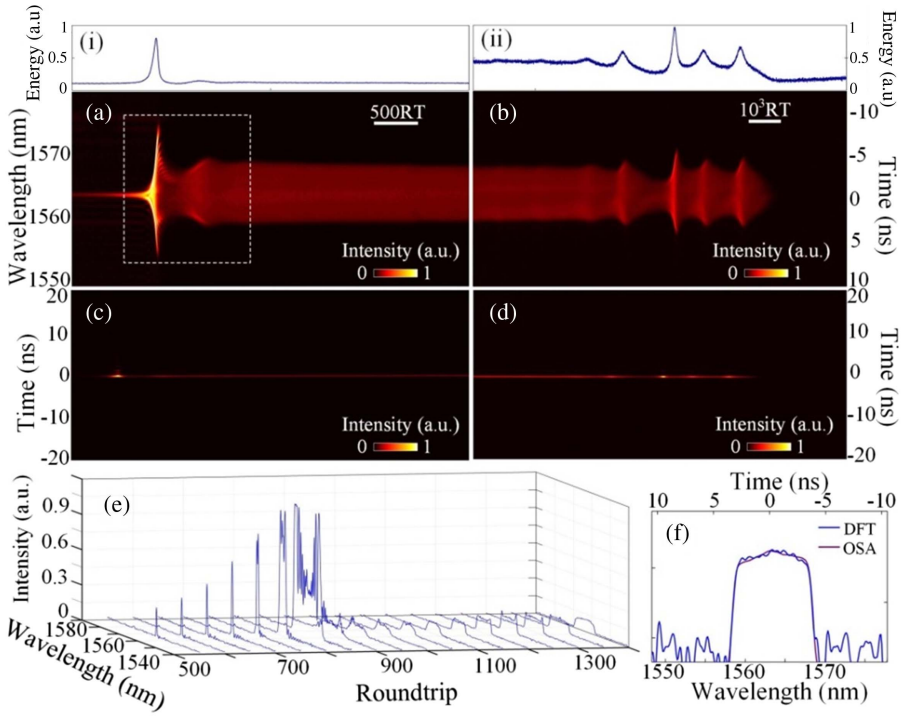

Fig. 7. Starting and shutting dynamics for the DS fiber laser. (a) Real-time spectral evolution dynamics during the starting of DSs. (b) Real-time spectral evolution dynamics during the shutting for DSs. (i) and (ii) show the energy evolution corresponding to (a) and (b), respectively. Experimental real-time observations without DFT for the (c) starting and (d) shutting processes correspond to (a) and (b), respectively. (e) Spectral evolution for the formation of DSs. The data are extracted from the square region in (a). (f) Optical spectra of DSs measured by the OSA and DFT technique.

NPR technique is utilized, extra unstable stages, such as *Q*-switched lasing, can be observed at the beginning of the build-up process [30,31]. The results have been verified with several previous works [25,30–32,38]. An SA can also influence the other behaviors of the starting and shutting processes. For example, the shutting process could be faster with larger nonsaturable absorption, while the fluctuation may be enhanced because larger pump power is needed. The starting and shutting processes would be shorter with larger modulation depth, and the fluctuation during the shutting process could be suppressed as well. However, the modulation depth should not be too large; otherwise, the *Q*-switch instability would be boosted in the oscillator.

Many factors can also influence birth and extinction dynamics, such as the dispersion map, pump power, turn-on and turn-off times, SA, and cavity structure. The variation of any one of these factors could change the birth and extinction behavior. Single-pulse mode-locking operation can be achieved within a certain range of pump powers. In this case, the effect of the variation in pump power is slight. With larger pump power, multiple pulses would be generated in a mode-locked laser. The birth and extinction dynamics would definitely be different [24,25,36]. The turn-on and turn-off times of the pump power could change the appearance of the build-up and shutting processes. A long turn-on time may lead to an unstable stage owing to the inadequate pump, and a long turn-off time would enhance fluctuation during the shutting process. Under a similar structure and dispersion map, the cavity length would not obviously influence birth and extinction dynamics. The variation in length of gain fiber would influence the behavior extremely. The difference in the build-up process between this work and Ref. [38] should be attributed to this factor. Actually, the mode-locked fiber laser is a complex dissipative system. It is generally the common interaction of several factors, which may induce some strange evolution dynamics. However, simple birth and extinction dynamics are needed from the application point.

We believe these results can further deepen understanding of the mode-locked fiber laser, and are helpful for laser design and applications. On one hand, the birth and extinction dynamics of CSs, SPs, and DSs are demonstrated in this work, which is more comprehensive by comparison to previous works. Dispersion management is generally used to obtain ultrafast pulses with different characteristics. This work is helpful to further distinguish and recognize the pulses under different dispersion maps, and to understand the effect of dispersion maps on pulse evolution, which is significant for laser design. On the other hand, the starting and shutting processes are extremely important in some applications, such as laser rapid processing, which needs to turn laser sources on and off repeatedly. The drastic outbursts in the starting and shutting would influence the processing quality seriously. This work can bring real-time insight into the management of laser reset.

Essentially, the birth and extinction dynamics are the response of mode-locked lasers to the switch of pump power. The increase of pump power induces relaxation oscillation

inevitably [39]. Meanwhile, saturable absorption drives the formation of ultrashort pulses from the noise background [19]. When the pump power is decreased, pulses decay correspondingly, but the remaining gain always drives the energy fluctuation. So relaxation oscillation, the interaction of picosecond and femtosecond pulses and fluctuation, can be generally observed during the starting and shutting processes. However, Q-switching, as well as relaxation oscillation can lead to the intense change in population inversion (or gain). So some phenomena under excessive pump power can be found, such as the transient complex spectrum broadening in this work and the transient bound state in Refs. [33,38].

4. CONCLUSION

By utilizing pump power as the triggering signal, the starting and shutting processes of CSs, SPs, and DSs are measured via the TS-DFT technique under different dispersion conditions. Relaxation oscillation can be observed in the build-up processes of CSs, SPs, and DSs benefitting from the use of an SWNT SA. However, the transition stage exhibits a distinct evolution pathway from relaxation oscillation to stable mode-locking operation. After the beating dynamics, the spectrum broadens with complex interaction of multiple pulses in a CS mode-locked fiber laser. SPs can form directly via beating dynamics, but a long instability is induced by relaxation oscillation. However, beating dynamics cannot be observed in the starting process of DSs. For the shutting process, CSs, SPs, and DSs also experience different dynamics and energy fluctuations. CSs vanish quickly, while SPs and DSs experience a long Q-switched fluctuation before extinction. The shutting process can also be influenced by the turn-off time. Here, the birth and extinction dynamics of CSs, SPs, and DSs in SWNT-mode-locked fiber lasers are revealed mainly experimentally, and the theoretical investigations need more attempts in further works. These findings provide new perspectives into the ultrafast transient dynamics and bring real-time insights into laser design and applications.

Funding. National Natural Science Foundation of China (NSFC) (11774310, 61525505, 61705193); China Postdoctoral Science Foundation (2017M610367).

Acknowledgment. We thank X. Yao, Y. Zhang, and W. Hu for fruitful discussions.

REFERENCES

1. J. Kim and Y. Song, "Ultralow-noise mode-locked fiber lasers and frequency combs: principles, status, and applications," Adv. Opt. Photon. **8**, 465–540 (2016).
2. G. Herink, B. Jalali, C. Ropers, and D. R. Solli, "Resolving the build-up of femtosecond mode-locking with single-shot spectroscopy at 90 MHz frame rate," Nat. Photonics **10**, 321–326 (2016).
3. C. Li, X. Wei, C. Kong, S. Tan, N. Chen, J. Kang, and K. K. Wong, "Fiber chirped pulse amplification of a short wavelength mode-locked thulium-doped fiber laser," APL Photon. **2**, 121302 (2017).
4. C. Jauregui, J. Limpert, and A. Tünnermann, "High-power fibre lasers," Nat. Photonics **7**, 861–867 (2013).
5. J. Ye and S. T. Cundiff, *Femtosecond Optical Frequency Comb: Principle, Operation and Applications* (Springer, 2005).
6. Y. Cui, F. Lu, and X. Liu, "Nonlinear saturable and polarization-induced absorption of rhenium disulfide," Sci. Rep. **7**, 40080 (2017).
7. F. W. Wise, A. Chong, and W. H. Renninger, "High-energy femtosecond fiber lasers based on pulse propagation at normal dispersion," Laser Photon. Rev. **2**, 58–73 (2008).
8. T. Hasan, Z. Sun, F. Wang, F. Bonaccorso, P. H. Tan, A. G. Rozhin, and A. C. Ferrari, "Nanotube-polymer composites for ultrafast photonics," Adv. Mater. **21**, 3874–3899 (2009).
9. X. X. Han, "Conventional soliton or stretched pulse delivered by nanotube-mode-locked fiber laser," Appl. Opt. **57**, 807–811 (2018).
10. D. Li, H. Jussila, Y. Wang, G. Hu, A. Tom, R. C. Howe, R. C. Howe, Z. Ren, J. Bai, T. Hasan, and Z. Sun, "Wavelength and pulse duration tunable ultrafast fiber laser mode-locked with carbon nanotubes," Sci. Rep. **8**, 2738 (2018).
11. X. Liu, "Hysteresis phenomena and multipulse formation of a dissipative system in a passively mode-locked fiber laser," Phys. Rev. A **81**, 023811 (2010).
12. S. Yamashita, "A tutorial on nonlinear photonic applications of carbon nanotube and graphene," J. Lightwave Technol. **30**, 427–447 (2012).
13. M. E. Fermann and I. Hartl, "Ultrafast fibre lasers," Nat. Photonics **7**, 868–874 (2013).
14. L. E. Nelson, D. J. Jones, K. Tamura, H. A. Haus, and E. P. Ippen, "Ultrashort-pulse fiber ring lasers," Appl. Phys. B **65**, 277–294 (1997).
15. P. Grelu and N. Akhmediev, "Dissipative solitons for mode-locked lasers," Nat. Photonics **6**, 84–92 (2012).
16. X. Liu, "Pulse evolution without wave breaking in a strongly dissipative-dispersive laser system," Phys. Rev. A **81**, 053819 (2010).
17. S. K. Turitsyn and E. G. Shapiro, "Dispersion-managed solitons in optical amplifier transmission systems with zero average dispersion," Opt. Lett. **23**, 682–684 (1998).
18. K. Kieu, W. H. Renninger, A. Chong, and F. W. Wise, "Sub-100 fs pulses at watt-level powers from a dissipative-soliton fiber laser," Opt. Lett. **34**, 593–595 (2009).
19. G. P. Agrawal, *Applications of Nonlinear Fiber Optics* (Academic, 2008).
20. E. P. Ippen, L. Y. Liu, and H. A. Haus, "Self-starting condition for additive-pulse mode-locked lasers," Opt. Lett. **15**, 183–185 (1990).
21. U. Keller, "Recent developments in compact ultrafast lasers," Nature **424**, 831–838 (2003).
22. H. Li, D. G. Ouzounov, and F. W. Wise, "Starting dynamics of dissipative-soliton fiber laser," Opt. Lett. **35**, 2403–2405 (2010).
23. A. Mahjoubfar, D. V. Churkin, S. Barland, N. Broderick, S. K. Turitsyn, and B. Jalali, "Time stretch and its applications," Nat. Photonics **11**, 341–351 (2017).
24. G. Herink, F. Kurtz, B. Jalali, D. R. Solli, and C. Ropers, "Real-time spectral interferometry probes the internal dynamics of femtosecond soliton molecules," Science **356**, 50–54 (2017).
25. X. Liu, X. Yao, and Y. Cui, "Real-time observation of the buildup of soliton molecules," Phys. Rev. Lett. **121**, 023905 (2018).
26. K. Krupa, K. Nithyanandan, U. Andral, P. Tchofo-Dinda, and P. Grelu, "Real-time observation of internal motion within ultrafast dissipative optical soliton molecules," Phys. Rev. Lett. **118**, 243901 (2017).
27. A. F. J. Runge, N. G. R. Broderick, and M. Erkintalo, "Observation of soliton explosions in a passively mode-locked fiber laser," Optica **2**, 36–39 (2015).
28. Z. Wang, Z. Wang, Y. Liu, R. He, J. Zhao, G. Wang, and G. Yang, "Self-organized compound pattern and pulsation of dissipative solitons in a passively mode-locked fiber laser," Opt. Lett. **43**, 478–481 (2018).
29. Y. Du, Z. Xu, and X. Shu, "Spatio-spectral dynamics of the pulsating dissipative solitons in a normal-dispersion fiber laser," Opt. Lett. **43**, 3602–3605 (2018).
30. P. Ryczkowski, M. Närhi, C. Billet, J. M. Merolla, G. Genty, and J. M. Dudley, "Real-time full-field characterization of transient dissipative soliton dynamics in a mode-locked laser," Nat. Photonics **12**, 221–227 (2018).

31. X. Wei, B. Li, Y. Yu, C. Zhang, and K. Tsia, "Unveiling multi-scale laser dynamics through time-stretch and time-lens spectroscopies," Opt. Express **25**, 29098–29120 (2017).
32. H. J. Chen, M. Liu, J. Yao, S. Hu, J. B. He, A. P. Luo, W. Xu, and Z. C. Luo, "Buildup dynamics of dissipative soliton in an ultrafast fiber laser with net-normal dispersion," Opt. Express **26**, 2972–2982 (2018).
33. J. Peng and H. Zeng, "Build-up of dissipative optical soliton molecules via diverse soliton interactions," Laser Photon. Rev. **12**, 1800009 (2018).
34. S. Hamdi, A. Coillet, and P. Grelu, "Real-time characterization of optical soliton molecule dynamics in an ultrafast thulium fiber laser," Opt. Lett. **43**, 4965–4968 (2018).
35. S. Sun, Z. Lin, W. Li, N. Zhu, and M. Li, "Time-stretch probing of ultra-fast soliton dynamics related to *Q*-switched instabilities in mode-locked fiber laser," Opt. Express **26**, 20888–20901 (2018).
36. Y. Yu, B. Li, X. Wei, Y. Xu, K. K. M. Tsia, and K. K. Y. Wong, "Spectral-temporal dynamics of multipulse mode-locking," Appl. Phys. Lett. **110**, 201107 (2017).
37. X. Liu, Y. Cui, D. Han, X. Yao, and Z. Sun, "Distributed ultrafast fibre laser," Sci. Rep. **5**, 9101 (2015).
38. X. M. Liu and Y. D. Cui, "Revealing the behavior of soliton buildup in a mode-locked laser," Adv. Photon. **1**, 016003 (2019).
39. O. Svelto, *Principles of Lasers* (Springer, 2010).
40. S. M. Kelly, "Characteristic sideband instability of periodically amplified average soliton," Electron. Lett. **28**, 806–807 (1992).